

# Robust Nonprehensile Object Transportation with Uncertain Inertial Parameters

Adam Heins and Angela P. Schoellig

**Abstract**—We consider the nonprehensile object transportation task known as the *waiter’s problem*—in which a robot must move an object on a tray from one location to another—when the transported object has uncertain inertial parameters. In contrast to existing approaches that completely ignore uncertainty in the inertia matrix or which only consider small parameter errors, we are interested in pushing the limits of the amount of inertial parameter uncertainty that can be handled. We first show how constraints that are robust to inertial parameter uncertainty can be incorporated into an optimization-based motion planning framework to transport objects while moving quickly. Next, we develop necessary conditions for the inertial parameters to be realizable on a bounding shape based on moment relaxations, allowing us to verify whether a trajectory will violate the constraints for *any* realizable inertial parameters. Finally, we demonstrate our approach on a mobile manipulator in simulations and real hardware experiments: our proposed robust constraints consistently successfully transport a 56 cm tall object with substantial inertial parameter uncertainty in the real world, while the baseline approaches drop the object while transporting it.

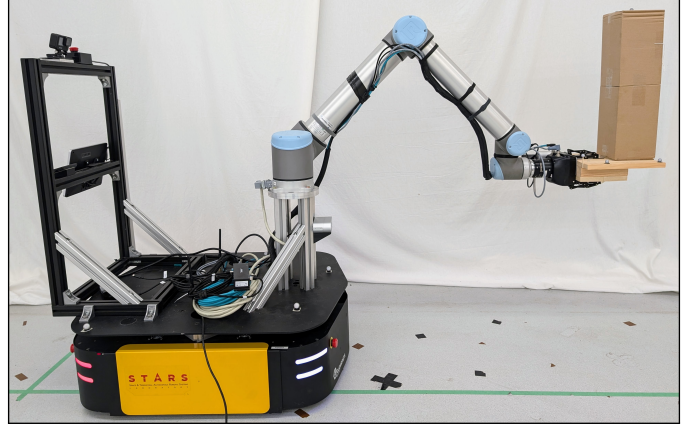


Figure 1: The goal of this work is to move an object on a tray to a desired position without dropping it, despite the inertial parameters of the object being uncertain. Here our mobile manipulator is transporting a tall box with uncertain contents. A video of our experiments is available at <http://tiny.cc/upright-robust>.

## I. INTRODUCTION

**T**HE *waiter’s problem* [1] is a nonprehensile manipulation task that requires a robot to transport objects from one location to another on a tray at the end effector (EE), like a restaurant waiter. This manipulation task is called *nonprehensile* [2] because the objects are not rigidly grasped: they are only attached to the robot by frictional contact and thus retain some independent degrees of freedom (DOFs). Other examples of nonprehensile manipulation include pushing, rolling, and throwing [3], [4]. A nonprehensile approach avoids grasping and ungrasping phases and can handle delicate or unwieldy objects which cannot be adequately grasped at all [5]; such an approach for transporting objects is useful in industries including food service, warehouse fulfillment, and manufacturing.

We build on our previous work on the waiter’s problem for mobile manipulators [6]. In contrast to [6], which focused on fast online replanning to react to dynamic obstacles while balancing objects with *known* properties, here we focus on

offline planning for a transported object with *unknown* inertial parameters—that is, the values of the mass, center of mass (CoM), and inertia matrix are not known exactly but rather lie in some set. Our approach is to plan trajectories to reach a desired EE position while satisfying constraints that ensure the transported object does not move with respect to the tray (see Fig. 1). These *sticking constraints* (so-called because they ensure the object “sticks” to the tray) depend on the geometric, frictional, and inertial properties of the object. The geometry of the object can in principle be estimated visually (e.g., using a camera), while frictional uncertainty can be reduced by using a high-friction material for the tray surface or by using a low friction coefficient in the planner [6]. However, the inertial properties can only be identified by moving the object around (see e.g. [7], [8]), which is time-consuming and could result in the object being dropped and damaged. Instead, we propose using *robust* constraints that successfully transport the object despite the presence of substantial inertial parameter uncertainty. Notably, we assume the CoM can be located at any height within the object, and that the inertia matrix can take any physically realizable value.

We focus on balancing a single tall object with known geometry but unknown mass and inertia matrix, and where the CoM is assumed to lie in a known polyhedral convex set. We use the object’s known geometry to constrain the set of possible inertial parameters. A set of inertial parameters can only be physically realized on a given shape if there exists a corresponding mass density function which is zero everywhere outside that shape [8]. We develop necessary conditions for the

This article was published in IEEE Robotics and Automation Letters. Digital Object Identifier (DOI): 10.1109/LRA.2025.3551067

This work was supported by the Natural Sciences and Engineering Research Council of Canada and the Canadian Institute for Advanced Research.

The authors are with the Learning Systems and Robotics Lab ([www.learnsyslab.org](http://www.learnsyslab.org)) at the Technical University of Munich, Germany, and the University of Toronto Institute for Aerospace Studies, Canada. They are also affiliated with the University of Toronto Robotics Institute, the Munich Institute of Robotics and Machine Intelligence (MIRMI), and the Vector Institute for Artificial Intelligence (e-mail: [adam.heins@robotics.utoronto.ca](mailto:adam.heins@robotics.utoronto.ca); [angela.schoellig@tum.de](mailto:angela.schoellig@tum.de)).

inertial parameters to be physically realizable on a bounding shape based on moment relaxations [9]. These realizability conditions allow us to verify that a planned trajectory does not violate the sticking constraints for *any* physically realizable value of the inertial parameters, providing theoretical guarantees for the robustness of our planned trajectories. In summary, the contributions of this work are:

- a planner for nonprehensile object transportation that explicitly handles objects with uncertain CoMs, extending the framework from [6];
- a theoretical analysis of the sticking constraint satisfaction in the presence of a bounded CoM and any physically realizable inertia matrix, based on moment relaxations [9];
- simulations and hardware experiments showing that our proposed robust constraints successfully transport the object—despite using tall objects with high inertial parameter uncertainty—while baseline approaches drop it;
- an open-source implementation of our planner, available at <https://github.com/utiasDSL/upright>.

## II. RELATED WORK

The waiter’s problem has been approached using a variety of methods including offline planning [5], [10]–[12], online planning (i.e., model predictive control) [6], [13], and reactive control [14]–[17]. Few of these approaches address inertial parameter uncertainty in the transported objects. One possible approach is to simulate the motion of a pendulum with the EE, which naturally minimizes lateral forces acting on the transported object without explicitly modelling it. However, so far this approach has only been used to minimize slosh when transporting liquids [14], [15] rather than (uncertain) rigid bodies. Another approach is [12], which develops a robust planner for the waiter’s problem based on reachability analysis, with parameter uncertainty represented using polynomial zonotopes. In contrast to our work, [12] focuses on small amounts of uncertainty (e.g., a 5% mass and inertia reduction) in both the transported objects and the links of the robot. The resulting trajectories are also quite slow, with negligible inertial acceleration (i.e., quasistatic). Instead, we achieve fast and dynamic motion with tall objects under high parameter uncertainty (i.e., CoMs located at any height in the object and *any* realizable inertia matrix), but we assume that uncertainty in the robot model is negligible (i.e., we use a well-calibrated industrial robot).

Our formulation of robust sticking constraints draws inspiration from legged robot balance control [18]–[21]. Indeed, the task of balancing an object on a tray is quite similar to balancing a legged robot represented with a reduced-order model, which uses the centroidal dynamics of the robot (i.e., the dynamics of a rigid body). In [19]–[21], the CoM of the robot is assumed to be uncertain and motions are generated that keep the robot balanced for any possible CoM value in a polyhedral set. In particular, we follow a similar approach to [21] for handling polyhedral CoM uncertainty by enforcing sticking constraints corresponding to a CoM located at each vertex of the set, and demonstrate its effectiveness for the waiter’s problem. In contrast to these approaches, however, we

are also interested in modelling and handling uncertainty in the inertia matrix. While the CoM can reasonably and intuitively be assumed to live in some convex polyhedral set, the inertia matrix is more complicated. When considering the inertia matrix, the set of physically realizable inertial parameters is *spectrahedral* (i.e., it can be represented using linear matrix inequalities (LMIs)) rather than polyhedral, as discussed in [8]. We develop necessary conditions for the inertial parameters to be physically realizable on a bounding shape, based on moment relaxations [9], which we use as constraints in a semidefinite program (SDP) to verify that our planned trajectories do not violate any sticking constraints despite inertial parameter uncertainty. Moment relaxations (i.e., Lasserre’s hierarchy) have previously been applied in robotics for tasks like certifiable localization [22] and trajectory planning [23], but not to bounds on the inertial parameters of a rigid body.

## III. BACKGROUND

We begin with mathematical notation and preliminaries.

### A. Notation

We denote the set of real numbers as  $\mathbb{R}$ , the non-negative reals as  $\mathbb{R}_+$ , the non-negative integers as  $\mathbb{N}$ , the  $n \times n$  symmetric matrices as  $\mathbb{S}^n$ , the symmetric positive semidefinite matrices as  $\mathbb{S}_+^n$ , and the symmetric positive definite matrices as  $\mathbb{S}_{++}^n$ . The notation  $\mathbf{A} \preceq \mathbf{B}$  means that  $\mathbf{B} - \mathbf{A} \in \mathbb{S}_+^n$ , while  $\leq$  denotes entry-wise inequality. The  $n \times n$  identity matrix is denoted  $\mathbf{1}_n$ . Finally, we use  $\text{diag}(\cdot)$  to construct (block) diagonal matrices.

### B. Polyhedron Double Description

Any convex polyhedron  $\mathcal{P}$  can be described as either the convex hull of its vertices or as a finite intersection of half spaces; this is called the *double description* of  $\mathcal{P}$ . When  $\mathcal{P}$  is also a cone, it is called a polyhedral convex cone (PCC) and can be described using either the *face* or *span* form [18]:

$$\begin{aligned} \mathcal{P} = \text{face}(\mathbf{U}) &= \{\mathbf{y} \mid \mathbf{U}\mathbf{y} \leq \mathbf{0}\} \\ &= \text{span}(\mathbf{V}) = \{\mathbf{V}\mathbf{z} \mid \mathbf{z} \geq \mathbf{0}\}. \end{aligned}$$

Following [24], we use the superscript  $(\cdot)^F$  to denote conversion from span to face form, such that  $\text{face}(\mathbf{U}^F) = \text{span}(\mathbf{U})$ , and we use  $(\cdot)^S$  to denote the conversion from face to span form. We perform the conversions using the `odd` library [25].

### C. Moment Relaxations

The *moment problem* asks when a sequence corresponds to the moments of some Borel measure. We will make use of SDP relaxations for the moment problem (*moment relaxations*), which we briefly summarize here from [9]. Define  $\mathbb{N}_d^n = \{\boldsymbol{\alpha} \in \mathbb{N}^n \mid \sum_{i=1}^n \alpha_i \leq d\}$ . Let  $\mathbf{r} \in \mathbb{R}^n$  be a point and let  $\boldsymbol{\alpha} \in \mathbb{N}_d^n$  be a vector of exponents applied elementwise, such that  $\mathbf{r}^{\boldsymbol{\alpha}} = r_1^{\alpha_1} \dots r_n^{\alpha_n}$ . Let  $f : \mathbb{R}^n \rightarrow \mathbb{R}$  be a polynomial of degree at most  $d$ . Then we can write  $f(\mathbf{r}) = \sum_{\boldsymbol{\alpha} \in \mathbb{N}_d^n} f_{\boldsymbol{\alpha}} \mathbf{r}^{\boldsymbol{\alpha}} = \mathbf{f}^T \mathbf{b}_d(\mathbf{r})$ , where  $\mathbf{f} = \{f_{\boldsymbol{\alpha}}\} \in \mathbb{R}^{s(d)}$  is the vector of the polynomial’s coefficients with size  $s(d) \triangleq \binom{n+d}{d}$  and  $\mathbf{b}_d(\mathbf{r}) = [1, r_1, \dots, r_n, r_1^2, r_1 r_2, \dots, r_n^d] \in \mathbb{R}^{s(d)}$  is the

basis vector for polynomials of degree at most  $d$  in graded lexicographical order. Given a vector  $\mathbf{z} = \{z_\alpha\} \in \mathbb{R}^{s(d)}$ , the *Riesz functional* associated with  $\mathbf{z}$  is  $L_{\mathbf{z}}(f) = \sum_{\alpha \in \mathbb{N}_d^n} f_\alpha z_\alpha$ , which maps a polynomial  $f : \mathbb{R}^n \rightarrow \mathbb{R}$  of degree  $d$  to a scalar value. Given a vector  $\mathbf{y} \in \mathbb{R}^{s(2d)}$ , the  $d$ th-order *moment matrix* associated with  $\mathbf{y}$  is  $\mathbf{M}_d(\mathbf{y}) = L_{\mathbf{y}}(\mathbf{b}_d(\mathbf{r})\mathbf{b}_d(\mathbf{r})^T) \in \mathbb{R}^{s(d) \times s(d)}$ , where  $L_{\mathbf{y}}$  is applied elementwise to each element of the matrix  $\mathbf{b}_d(\mathbf{r})\mathbf{b}_d(\mathbf{r})^T$ , such that the element  $\mathbf{r}^\alpha \mathbf{r}^\beta = \mathbf{r}^{\alpha+\beta}$ , with  $\alpha, \beta \in \mathbb{N}_d^n$ , is mapped to the value  $y_{\alpha+\beta}$ . In addition, given a polynomial  $p : \mathbb{R}^n \rightarrow \mathbb{R}$  of degree  $2d$ , the *localizing matrix* associated with  $p$  and  $\mathbf{y}$  is  $\mathbf{M}_d(p\mathbf{y})$ .

Suppose we want to determine if a given sequence  $\mathbf{y} \in \mathbb{R}^{s(2d)}$ , known as a *truncated moment sequence (TMS)*, represents the moments of some Borel measure  $\gamma$  supported in a compact semialgebraic set  $\mathcal{K} = \{\mathbf{r} \in \mathbb{R}^n \mid p_j(\mathbf{r}) \geq 0, j = 1, \dots, n_p\}$ , where each  $p_j(\mathbf{r})$  is a polynomial with degree  $2v_j$  (even) or  $2v_j - 1$  (odd). That is, we want to know if there exists  $\gamma : \mathbb{R}^n \rightarrow \mathbb{R}_+$  such that

$$\mathbf{M}_d(\mathbf{y}) = \int_{\mathcal{K}} \mathbf{b}_d(\mathbf{r})\mathbf{b}_d(\mathbf{r})^T d\gamma(\mathbf{r}),$$

which is known as the *truncated K-moment problem (TKMP)*. Define  $p_0(\mathbf{r}) = 1$  with  $v_0 = 0$ . Then a necessary condition for  $\gamma$  to exist (see Theorem 3.8 of [9]) is that for any  $r \geq d$ , we can extend  $\mathbf{y} \in \mathbb{R}^{s(2d)}$  to  $\tilde{\mathbf{y}} \in \mathbb{R}^{s(2r)}$  while satisfying

$$\mathbf{M}_{r-v_j}(p_j \tilde{\mathbf{y}}) \succcurlyeq \mathbf{0}, \quad j = 0, \dots, n_p. \quad (1)$$

The moment constraints (1) become tighter as  $r$  increases, forming a hierarchy of SDP relaxations for the TKMP.

#### IV. MODELLING

Next, we present the models of the robot and object.

##### A. Robot Model

As in [6], we consider a velocity-controlled mobile manipulator with state  $\mathbf{x} = [\mathbf{q}^T, \boldsymbol{\nu}^T, \dot{\boldsymbol{\nu}}^T]^T \in \mathbb{R}^{n_x}$ , where  $\mathbf{q}$  is the generalized position, which includes the planar pose of the mobile base and the arm's joint angles, and  $\boldsymbol{\nu}$  is the generalized velocity. The input  $\mathbf{u} \in \mathbb{R}^{n_u}$  is the generalized jerk. We use a kinematic model, which we represent generically as  $\dot{\mathbf{x}} = \mathbf{a}(\mathbf{x}) + \mathbf{B}(\mathbf{x})\mathbf{u}$ , with  $\mathbf{a}(\mathbf{x}) \in \mathbb{R}^{n_x}$  and  $\mathbf{B}(\mathbf{x}) \in \mathbb{R}^{n_x \times n_u}$ . Though the actual commands sent to the robot are velocities, including acceleration and jerk in the model allows us to reason about the sticking constraints and encourage smoothness.

##### B. Object Model

We model the transported object as a rigid body subject to the Newton-Euler equations

$$\mathbf{w}_C = \mathbf{w}_{GI}, \quad (2)$$

where  $\mathbf{w}_C$  is the contact wrench (CW) and  $\mathbf{w}_{GI}$  is the gravito-inertial wrench (GIW). All quantities are expressed in a frame attached to the EE. We have

$$\mathbf{w}_{GI} \triangleq \boldsymbol{\Xi}\boldsymbol{\eta} - \text{ad}(\boldsymbol{\xi})^T \boldsymbol{\Xi}\boldsymbol{\xi}, \quad (3)$$

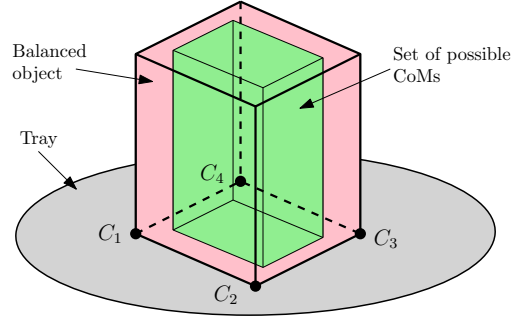


Figure 2: A box (red) on a tray, with four contact points  $C_1$ – $C_4$  located at the vertices of the base. We assume that the box's center of mass (CoM) is not known exactly, but rather only known to lie inside some polyhedral set (green).

where  $\boldsymbol{\Xi} \in \mathbb{S}_+^6$  is the object's spatial mass matrix,  $\boldsymbol{\xi} = [\boldsymbol{\omega}^T, \mathbf{v}^T]^T$  is the spatial velocity with angular component  $\boldsymbol{\omega} \in \mathbb{R}^3$  and linear component  $\mathbf{v} \in \mathbb{R}^3$ ,

$$\text{ad}(\boldsymbol{\xi}) \triangleq \begin{bmatrix} \boldsymbol{\omega}^\times & \mathbf{0} \\ \mathbf{v}^\times & \boldsymbol{\omega}^\times \end{bmatrix}$$

is the adjoint of  $\boldsymbol{\xi}$  with  $(\cdot)^\times$  forming a skew-symmetric matrix such that  $\mathbf{a}^\times \mathbf{b} = \mathbf{a} \times \mathbf{b}$  for any  $\mathbf{a}, \mathbf{b} \in \mathbb{R}^3$ , and  $\boldsymbol{\eta} = [\dot{\boldsymbol{\omega}}^T, \dot{\mathbf{v}}^T - \mathbf{g}^T]^T$  with gravitational acceleration  $\mathbf{g} \in \mathbb{R}^3$ . The mass matrix is defined as

$$\boldsymbol{\Xi} \triangleq \begin{bmatrix} \mathbf{I} & m\mathbf{c}^\times \\ -m\mathbf{c}^\times & m\mathbf{1}_3 \end{bmatrix},$$

where  $m$  is the object's mass,  $\mathbf{c}$  is the position of the object's CoM, and  $\mathbf{I}$  is its inertia matrix.

#### V. ROBUST STICKING CONSTRAINTS

We want to enforce constraints on the robot's motion so that the transported object does not move relative to the EE (i.e., it "sticks" to the EE). These sticking constraints prevent the object from sliding, tipping, or breaking contact. This is known as a *dynamic grasp* [26].

##### A. Contact Force Constraints

We can ensure an object sticks to the EE by including all contact forces directly into the motion planner and constraining the solution to be consistent with the desired (sticking) dynamics. Suppose there are  $n_c$  contact points  $\{C_i\}_{i=1}^{n_c}$  between the object and tray (see Fig. 2), with corresponding contact forces  $\{\mathbf{f}_i\}_{i=1}^{n_c}$ . By Coulomb's law, each contact force  $\mathbf{f}_i \in \mathbb{R}^3$  must lie inside its friction cone, which we linearize to obtain the set of constraints  $\mathbf{F}_i \mathbf{f}_i \leq \mathbf{0}$ , where

$$\mathbf{F}_i = \begin{bmatrix} 0 & 0 & -1 \\ 1 & 1 & -\mu_i \\ 1 & -1 & -\mu_i \\ -1 & 1 & -\mu_i \\ -1 & -1 & -\mu_i \end{bmatrix} [\hat{\mathbf{t}}_{i_1} \quad \hat{\mathbf{t}}_{i_2} \quad \hat{\mathbf{n}}_i]^T,$$

with friction coefficient  $\mu_i$ , contact normal  $\hat{\mathbf{n}}_i$ , and orthogonal contact tangent directions  $\hat{\mathbf{t}}_{i_1}$  and  $\hat{\mathbf{t}}_{i_2}$ . Letting  $\boldsymbol{\zeta} = [\mathbf{f}_1^T, \dots, \mathbf{f}_{n_c}^T]^T$ , we can write the linearized friction cone constraints for all  $n_c$  contact forces in matrix form as

$$\mathbf{F}\boldsymbol{\zeta} \leq \mathbf{0}, \quad (4)$$

where  $\mathbf{F} = \text{diag}(\mathbf{F}_1, \dots, \mathbf{F}_{n_c})$ . The CW on the object is

$$\mathbf{w}_C \triangleq \begin{bmatrix} \boldsymbol{\tau}_C \\ \mathbf{f}_C \end{bmatrix} = \sum_{i=1}^{n_c} \mathbf{G}_i \mathbf{f}_i, \quad (5)$$

where  $\boldsymbol{\tau}_C$  and  $\mathbf{f}_C$  are the total contact torque and force and  $\mathbf{G}_i = [-\mathbf{r}_i^x, \mathbf{1}_3]^T$  is the  $i$ th contact Jacobian with  $\mathbf{r}_i$  the location of  $C_i$ . The object sticks to the EE at a given time instant if a set of contact forces can be found satisfying (2)–(5). This approach can handle any number of (possibly non-coplanar) contact points, with surface contacts represented as polygons with a contact point at each vertex.

The set  $\mathcal{W}_C$  of all possible contact wrenches is known as the *contact wrench cone* (CWC) [18], which is a PCC containing all CWs that can be produced by feasible contact forces. We have  $\mathcal{W}_C = \{\mathbf{G}\boldsymbol{\zeta} \mid \mathbf{F}\boldsymbol{\zeta} \leq \mathbf{0}\}$ , where  $\mathbf{G} = [\mathbf{G}_1, \dots, \mathbf{G}_{n_c}]$  is known as the *grasp matrix*. From (2), we must have  $\mathbf{w}_{\text{GI}} \in \mathcal{W}_C$  for the object to remain stationary relative to the EE.

### B. Robustness to Inertial Parameter Uncertainty

Let  $\boldsymbol{\theta} = [m, m\mathbf{c}^T, \text{vech}(\mathbf{I})^T]^T \in \mathbb{R}^{10}$  be the inertial parameter vector for the object, where  $\text{vech}(\mathbf{I}) \in \mathbb{R}^6$  is the *half-vectorization* of  $\mathbf{I}$  [7]. Furthermore, let us assume that the exact value of  $\boldsymbol{\theta}$  is unknown, but that it lies inside a set  $\Theta$ . Since  $\mathbf{w}_{\text{GI}}$  is linear in  $\boldsymbol{\theta}$  [7], we can write the set of possible GIWs under inertial parameter uncertainty as

$$\mathcal{W}_{\text{GI}}(\boldsymbol{\xi}, \boldsymbol{\eta}) = \{\mathbf{Y}(\boldsymbol{\xi}, \boldsymbol{\eta})\boldsymbol{\theta} \mid \boldsymbol{\theta} \in \Theta\}$$

where  $\mathbf{Y}(\boldsymbol{\xi}, \boldsymbol{\eta}) \in \mathbb{R}^{6 \times 10}$  is known as the *regressor matrix*. To ensure the sticking constraints are satisfied for any  $\boldsymbol{\theta} \in \Theta$ , we want to generate EE motions  $(\boldsymbol{\xi}, \boldsymbol{\eta})$  that satisfy

$$\mathcal{W}_{\text{GI}}(\boldsymbol{\xi}, \boldsymbol{\eta}) \subseteq \mathcal{W}_C \quad (6)$$

at all timesteps. More concretely, (6) is satisfied if and only if, for each  $\boldsymbol{\theta} \in \Theta$ , there exists a set of contact forces  $\boldsymbol{\zeta}$  satisfying  $\mathbf{Y}(\boldsymbol{\xi}, \boldsymbol{\eta})\boldsymbol{\theta} = \mathbf{G}\boldsymbol{\zeta}$  and  $\mathbf{F}\boldsymbol{\zeta} \leq \mathbf{0}$ .

We can enforce (6) using only constraints on the extreme points  $\text{ex}(\Theta)$  of  $\Theta$ . To see this, observe that since  $\mathcal{W}_C$  is convex, any convex combination of points in  $\mathcal{W}_C$  also lies in  $\mathcal{W}_C$ . And since any  $\boldsymbol{\theta} \in \Theta$  is a convex combination of points in  $\text{ex}(\Theta)$ , it follows that  $\mathbf{Y}(\boldsymbol{\xi}, \boldsymbol{\eta})\boldsymbol{\theta} \in \mathcal{W}_C$  for any  $\boldsymbol{\theta} \in \Theta$  as long as  $\mathbf{Y}(\boldsymbol{\xi}, \boldsymbol{\eta})\hat{\boldsymbol{\theta}} \in \mathcal{W}_C$  for all  $\hat{\boldsymbol{\theta}} \in \text{ex}(\Theta)$ .

Furthermore, for lightweight objects, we can ignore the value of the object’s mass when transporting a single object.<sup>1</sup> To see this, suppose the true inertial parameter vector is  $\boldsymbol{\theta} = [m, m\mathbf{c}^T, \text{vech}(\mathbf{I})^T]^T \in \Theta$ . Since  $\mathcal{W}_C$  is a convex cone and  $m > 0$ , it follows that  $\mathbf{Y}(\boldsymbol{\xi}, \boldsymbol{\eta})\boldsymbol{\theta} \in \mathcal{W}_C$  if and only if  $\mathbf{Y}(\boldsymbol{\xi}, \boldsymbol{\eta})\hat{\boldsymbol{\theta}} \in \mathcal{W}_C$ , where  $\hat{\boldsymbol{\theta}} \triangleq \boldsymbol{\theta}/m$  is the *mass-normalized* parameter vector. In other words, for any  $\boldsymbol{\theta} \in \Theta$ , we can always instead use  $\hat{\boldsymbol{\theta}}$  to enforce the sticking constraints, which is independent of the true mass. This result holds for any object that is not in contact with any others (except of course the tray). However, when multiple objects are in contact with each other, the force transmitted between them depends on their relative masses, so we can no longer ignore them.

<sup>1</sup>We are assuming that the object has a small enough mass for the robot’s internal position controller to accurately track the desired trajectory despite the uncertain payload.

Finally, we will also ignore uncertainty in the inertia matrix *while planning* trajectories, as it would be expensive to enforce the LMI constraint required for physical realizability [8]. Instead, we will check our trajectories *after planning* to verify that the sticking constraints are satisfied for any physically realizable inertial parameters—our experiments suggest that handling large uncertainty in the CoM gives us enough robustness to handle any physically realizable inertia matrix as well. We will return to the analysis of physically realizable inertial parameters in Sec. VII. For now, since we are ignoring uncertainty in the mass and inertia matrix, we are left with uncertainty in the CoM. Similar to [21], our approach therefore is to assume that  $\mathbf{c}$  belongs to a known polyhedral set  $\mathcal{C}$  with  $n_v$  vertices (see Fig. 2) and enforcing sticking constraints for  $n_v$  objects, which differ only in that the  $i$ th object has CoM located at the  $i$ th vertex of the CoM uncertainty set. This is equivalent to enforcing (6).

## VI. ROBUST PLANNING

Our goal is to generate a state-input trajectory for our robot that satisfies the robust sticking constraints developed in the previous section. We formulate the motion planning problem as a constrained optimal control problem (OCP), similar to the formulation in [6]. In contrast to [6], however, which solves the OCP online in a model predictive control framework, we solve it once offline with a longer time horizon and then track the resulting optimal trajectory; we found this approach to be more reliable in our experiments. In particular, we found that a longer time horizon converged to the desired position faster with fewer oscillations, and that updating the desired trajectory online could cause additional EE vibration that made it more likely for tall, uncertain objects to be dropped. The trajectories  $\mathbf{x}(t)$ ,  $\mathbf{u}(t)$ , and  $\boldsymbol{\zeta}(t)$  are optimized over a duration  $T$  by solving a nonlinear optimization problem. Suppressing the time dependencies, the problem is

$$\begin{aligned} & \underset{\mathbf{x}, \mathbf{u}, \boldsymbol{\zeta}}{\text{argmin}} && \frac{1}{2} \int_0^T \ell(\mathbf{x}, \mathbf{u}) dt \\ & \text{subject to} && \dot{\mathbf{x}} = \mathbf{a}(\mathbf{x}) + \mathbf{B}(\mathbf{x})\mathbf{u} \quad (\text{robot model}) \\ & && \mathcal{W}_{\text{GI}}(\mathbf{x}) \subseteq \mathcal{W}_C \quad (\text{sticking}) \quad (7) \\ & && \mathbf{x} \leq \mathbf{x} \leq \bar{\mathbf{x}} \quad (\text{state limits}) \\ & && \mathbf{u} \leq \mathbf{u} \leq \bar{\mathbf{u}} \quad (\text{input limits}) \\ & && \boldsymbol{\varphi}(\mathbf{x}_f) = \mathbf{0} \quad (\text{terminal}) \end{aligned}$$

where the stage cost is

$$\ell(\mathbf{x}, \mathbf{u}) = \|\Delta\mathbf{r}(\mathbf{x})\|_{\mathbf{W}_r}^2 + \|\mathbf{x}\|_{\mathbf{W}_x}^2 + \|\mathbf{u}\|_{\mathbf{W}_u}^2,$$

with  $\|\cdot\|_{\mathbf{W}}^2 = (\cdot)^T \mathbf{W} (\cdot)$  for weight matrix  $\mathbf{W}$ , and  $\Delta\mathbf{r}(\mathbf{x}) = \mathbf{r}_d - \mathbf{r}_e(\mathbf{x})$  is the EE position error between the desired position  $\mathbf{r}_d$  and the current position  $\mathbf{r}_e(\mathbf{x})$ . The sticking constraints implicitly depend on the contact forces  $\boldsymbol{\zeta}$ , and we have expressed  $\mathcal{W}_{\text{GI}}$  as a function of  $\mathbf{x}$  via forward kinematics. The terminal constraint  $\boldsymbol{\varphi}(\mathbf{x}_f) = [\Delta\mathbf{r}(\mathbf{x}_f)^T, \boldsymbol{\nu}_f^T, \dot{\boldsymbol{\nu}}_f^T]^T = \mathbf{0}$  acts only on the final state  $\mathbf{x}_f \triangleq \mathbf{x}(T)$  and steers it toward a stationary state with no position error.

We solve (7) by discretizing the planning horizon  $T$  with a fixed timestep  $\Delta t$  and using sequential quadratic programming

(SQP) via the open-source framework OCS2 [27] and quadratic programming solver HPIPM [28], with required Jacobians computed using automatic differentiation. We use the Gauss-Newton approximation for the Hessian of the cost and we soften all state limits and sticking constraints: given a generic state constraint  $g(\mathbf{x}) \geq 0$ , we add a slack variable  $s \geq 0$  to relax the constraint to  $g(\mathbf{x}) + s \geq 0$ , and the  $L_2$  penalty  $w_s s^2$  is added to the cost with weight  $w_s > 0$ . Like [6], we also plan while assuming that there is *zero* contact friction between the tray and transported object (i.e., tangential forces are to be avoided, but small ones are allowed because the constraints are soft). This provides robustness to uncertain friction and other disturbances while also reducing the computational cost of solving (7), since each contact force variable need only be represented by a single non-negative scalar representing the normal force (see [6] for more details). Given the soft constraints and time discretization of (7), robust sticking is not *guaranteed* but is heavily *encouraged*.

Once we have solved (7) to obtain the planned optimal trajectory  $\mathbf{x}_d(t) = [\mathbf{q}_d^T(t), \boldsymbol{\nu}_d^T(t), \dot{\boldsymbol{\nu}}_d^T(t)]^T$ , we need to track it online. At each control timestep, we generate the commanded velocity  $\boldsymbol{\nu}_{\text{cmd}}$  using the simple affine control law  $\boldsymbol{\nu}_{\text{cmd}} = \mathbf{K}_p(\mathbf{q}_d - \mathbf{q}) + \boldsymbol{\nu}_d$ , where  $\mathbf{K}_p \in \mathbb{S}_{++}^9$  is a gain matrix.

## VII. VERIFYING STICKING CONSTRAINT SATISFACTION

Let us now consider uncertainty in the inertia matrix. We want a way to show that our choice to ignore inertia matrix uncertainty in the planner is justified; that is, given a trajectory, we want to verify that the sticking constraints are not violated for *any* realizable value of the inertia matrix. In this section we develop an SDP to determine an upper bound on the maximum constraint violation given the uncertain inertial parameters and bounding shape for the object.

### A. Double Description of the Contact Wrench Cone

Following [18], we build the face form of the CWC. First, notice that (4) describes a PCC face( $\mathbf{F}$ ). Converting (4) to span form, we have  $\mathcal{W}_C = \{\mathbf{G}\mathbf{F}^S \mathbf{z} \mid \mathbf{z} \geq \mathbf{0}\}$ . Next, letting  $\mathbf{H} = (\mathbf{G}\mathbf{F}^S)^F \in \mathbb{R}^{n_h \times 6}$ , we have the face form of the CWC  $\mathcal{W}_C = \{\mathbf{w} \in \mathbb{R}^6 \mid \mathbf{H}\mathbf{w} \leq \mathbf{0}\}$ . This form allows us to write the robust sticking constraints (6) as

$$\mathbf{H}\mathbf{Y}(\boldsymbol{\xi}, \boldsymbol{\eta})\boldsymbol{\theta} \leq \mathbf{0} \quad \forall \boldsymbol{\theta} \in \Theta. \quad (8)$$

Let  $\mathbf{h}_i^T$  be the  $i$ th row of  $\mathbf{H}$ . Then we can rewrite the constraint (8) as a set of inner optimization problems

$$\left( \max_{\boldsymbol{\theta} \in \Theta} \mathbf{h}_i^T \mathbf{Y}(\boldsymbol{\xi}, \boldsymbol{\eta})\boldsymbol{\theta} \right) \leq 0, \quad (9)$$

with one problem for each of the  $n_h$  rows. This inequality form of the sticking constraints will allow us to solve for the worst-case value of each constraint. However, we first need to determine appropriate bounds on the set  $\Theta$ .

### B. Worst-Case Sticking Constraints

Let us apply the moment relaxation machinery from Sec. III-C to the problem of physically realizable inertial

parameters. We have dimension  $n = 3$  and degree  $d = 1$ . The TMS  $\mathbf{y} \in \mathbb{R}^{10}$  and the associated moment matrix  $\mathbf{M}_1(\mathbf{y})$  can be used to represent the inertial parameters of a rigid body, with the relationship

$$\mathbf{M}_1(\mathbf{y}) = \begin{bmatrix} m & m\mathbf{c}^T \\ m\mathbf{c} & \mathbf{S} \end{bmatrix}, \quad (10)$$

where  $\mathbf{S} = (1/2)\text{tr}(\mathbf{I})\mathbf{1}_3 - \mathbf{I}$  [8].<sup>2</sup> We want to constrain the inertial parameters to correspond to a mass density  $\rho : \mathbb{R}^3 \rightarrow \mathbb{R}_+$  supported entirely in a compact bounding shape  $\mathcal{K} = \{\mathbf{r} \in \mathbb{R}^3 \mid p_j(\mathbf{r}) \geq 0, j = 1, \dots, n_p\}$  that contains the transported object, where each  $p_j$  is a polynomial of degree  $2v_j$  or  $2v_j - 1$ , such that

$$\mathbf{M}_1(\mathbf{y}) = \int_{\mathcal{K}} \mathbf{b}_1(\mathbf{r})\mathbf{b}_1(\mathbf{r})^T d\rho(\mathbf{r}).$$

For simplicity, we assume our bounding shape is a convex polyhedron, so  $v_j = 1$  for each  $j = 1, \dots, n_p$ , and we take  $p_0(\mathbf{r}) = 1$  with  $v_0 = 0$ . Given an EE trajectory, we want to determine if any realizable value of the inertial parameters would violate the sticking constraints (9) at any time. That is, we would like to know if the optimal value of

$$\max_{\boldsymbol{\theta} \in \Theta} \mathbf{h}_i^T \mathbf{Y}(\boldsymbol{\xi}, \boldsymbol{\eta})\boldsymbol{\theta} \quad (11)$$

is positive for any row  $\mathbf{h}_i^T$  of  $\mathbf{H}$  at any time instant of the trajectory. Using the conditions (1) with order  $r = 2$ , the problem (11) can be relaxed to the SDP

$$\begin{aligned} & \max_{\boldsymbol{\theta}, \tilde{\mathbf{y}}} \mathbf{h}_i^T \mathbf{Y}(\boldsymbol{\xi}, \boldsymbol{\eta})\boldsymbol{\theta} \\ & \text{subject to} \quad \mathbf{M}_1(\tilde{\mathbf{y}}) = \begin{bmatrix} 1 & \mathbf{c}(\boldsymbol{\theta})^T \\ \mathbf{c}(\boldsymbol{\theta}) & \mathbf{S}(\boldsymbol{\theta}) \end{bmatrix}, \\ & \quad \mathbf{M}_{2-v_j}(p_j \tilde{\mathbf{y}}) \succcurlyeq \mathbf{0}, \quad j = 0, \dots, n_p, \\ & \quad \mathbf{c}(\boldsymbol{\theta}) \in \mathcal{C}, \end{aligned} \quad (12)$$

where  $\tilde{\mathbf{y}} \in \mathbb{R}^{20}$  is an extended TMS, we have constrained the CoM  $\mathbf{c}$  to be located within some convex polyhedron  $\mathcal{C} \subset \mathcal{K}$ , and we have fixed  $m = 1$  since the sticking constraints are independent of mass for a single object. We have also made the dependencies on the decision variable  $\boldsymbol{\theta}$  explicit for clarity; note that  $\mathbf{S}$  and  $\mathbf{c}$  depend linearly on  $\boldsymbol{\theta}$ .

Since (12) is a relaxation of (11), its optimal value is an upper bound on the maximum possible violation for each constraint. Notably, (12) accounts for all possible values of the inertia matrix. We verify that a planned trajectory is robust to inertial parameter uncertainty by solving (12) pointwise at a fixed frequency along the trajectory. If the optimal value of (12) is always non-positive, then the constraint is not violated; we assume that the time discretization is fine enough that the constraints are not violated between timesteps. Furthermore, we can verify robustness to uncertain friction coefficients at the same time by constructing  $\mathcal{W}_C$  and thus  $\mathbf{H}$  with low friction coefficients: if the constraints are never violated, then any combination of higher friction coefficients and realizable inertial parameters will also satisfy the constraints.

<sup>2</sup>A permuted version of (10), known as the *pseudo-inertia matrix*, is the more common form in the robot dynamics literature (see e.g. [8]), but here we maintain consistency with the TKMP literature [9].

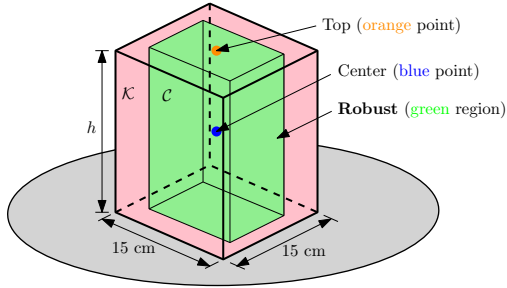


Figure 3: We transport a cuboid-shaped object  $\mathcal{K}$  (red) with an uncertain CoM contained in  $\mathcal{C}$  (green). We test three variations of the sticking constraints: assume the CoM is at the object's centroid (Center), assume it is centered at the top of the object (Top), and Robust, in which the controller enforces sticking constraints for eight different objects, where each has its CoM at one of the vertices of  $\mathcal{C}$ .

One could also consider enforcing full realizability constraints directly in the planning problem (7) to ensure the planned trajectories are robust a priori. However, this would be computationally expensive and numerically challenging because of the LMI constraints required for physical realizability combined with the nonlinearity of the problem. We leave this for future work.

## VIII. SIMULATION EXPERIMENTS

We begin the evaluation of our proposed robust planning approach in simulation using the PyBullet simulator and a simulated version of our experimental platform, a 9-DOF mobile manipulator consisting of a Ridgeback mobile base and UR10 arm, shown in Fig. 1. In all experiments (simulated and real) we use  $\Delta t = 0.1$  s,  $T = 10$  s, and weights

$$\begin{aligned} \mathbf{W}_r &= \mathbf{1}_3, & \mathbf{W}_x &= \text{diag}(0\mathbf{1}_9, 10^{-1}\mathbf{1}_9, 10^{-2}\mathbf{1}_9), \\ \mathbf{W}_u &= 10^{-3}\mathbf{1}_9, & w_s &= 100. \end{aligned}$$

The state and input limits are

$$\bar{\mathbf{q}} = \begin{bmatrix} 10e_3 \\ 2\pi e_6 \end{bmatrix}, \quad \bar{\mathbf{v}} = \begin{bmatrix} 1.1e_2 \\ 2e_3 \\ 3e_4 \end{bmatrix}, \quad \dot{\bar{\mathbf{v}}} = \begin{bmatrix} 2.5e_2 \\ 1 \\ 10e_6 \end{bmatrix}, \quad \bar{\mathbf{u}} = \begin{bmatrix} 20e_3 \\ 80e_6 \end{bmatrix},$$

where  $\bar{\mathbf{x}} = [\bar{\mathbf{q}}^T, \bar{\mathbf{v}}^T, \dot{\bar{\mathbf{v}}}^T]^T$ ,  $\mathbf{x} = -\bar{\mathbf{x}}$ ,  $\mathbf{u} = -\bar{\mathbf{u}}$ , and  $e_n$  denotes an  $n$ -dimensional vector of ones. The control gain is  $\mathbf{K}_p = \mathbf{1}_9$  and the simulation timestep is 0.1 ms. All experiments are run on a standard laptop with eight Intel Xeon CPUs at 3 GHz and 16 GB of RAM.

We are interested in cases where the inertial parameters of the transported object are uncertain and this uncertainty can result in task failures (i.e., the object is dropped) if the uncertainty is ignored. We use a tall box  $\mathcal{K}$  with a 15 cm  $\times$  15 cm base and height  $h$  (see Fig. 3) as the transported object. This object is tall relative to its support area and therefore prone to tipping over, particularly if the inertial parameters are not known exactly. Suppose we assume that the CoM can lie anywhere in a box  $\mathcal{C}$  with dimensions 12 cm  $\times$  12 cm  $\times$   $h$ , centered within  $\mathcal{K}$ ; that is, the CoM can be located *anywhere* in the object as long as it is at least 1.5 cm from the sides. The simulated friction coefficient between the box and tray is  $\mu = 0.2$ . We compare three sets of sticking constraints (again, see Fig. 3):

- **Center:** The CoM is located at the center of  $\mathcal{C}$ ;

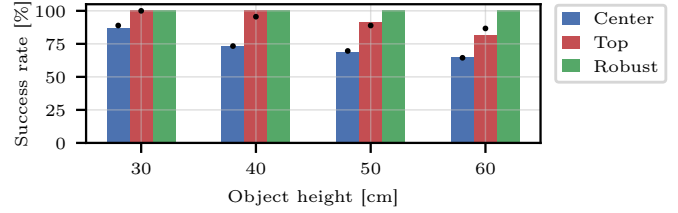


Figure 4: Success rate of the different types of sticking constraints for all 135 combinations of desired positions, CoMs, and inertias for each object height and constraint method (1620 total runs). The Robust constraints always successfully transport the object, while the other constraint types result in an increasing number of failures as the object height increases; the rate varies slightly with the number of SQP iterations  $n_s$ . Here the bar shows  $n_s = 3$  and the black dot  $n_s = 10$ .

- **Top:** The CoM is centered on the top face of  $\mathcal{C}$ ;
- **Robust:** A set of eight sticking constraints are used, corresponding to a CoM at each vertex of  $\mathcal{C}$ .

In all cases, the inertia matrix used in the planner is set to correspond to a uniform mass density. The first two constraint methods are baselines where we are not explicitly accounting for the uncertainty in the parameters. Intuitively, it is more difficult to transport an object with a higher CoM, so we may expect the Top constraints to be more successful than the Center constraints. In contrast to these baselines, our proposed Robust constraints explicitly handle uncertainty in the CoM.

We test all combinations of the following: three desired positions  $\mathbf{r}_{d_1} = [-2, 1, 0]^T$ ,  $\mathbf{r}_{d_2} = [0, 2, 0.25]^T$ , and  $\mathbf{r}_{d_3} = [2, 0, -0.25]^T$  (in meters), 15 different simulated CoM positions (one at the center of  $\mathcal{C}$ , eight at the vertices of  $\mathcal{C}$ , and six at the centers of the faces of  $\mathcal{C}$ ), and three different values for the inertia matrix, computed as follows. We solve a convex optimization problem to find the diagonal inertia matrix about the CoM which corresponds to a set of point masses at the vertices of  $\mathcal{K}$  with the maximum smallest eigenvalue. This gives us a large realizable inertia matrix value  $\mathbf{I}$ ; we then also test with the smaller inertia values  $0.5\mathbf{I}$  and  $0.1\mathbf{I}$ . The simulated mass is fixed to  $m = 1$  kg. We test each of the 135 total combinations of trajectory, CoM, and inertia matrix for different object heights  $h$  and constraint methods.

The success rates for the simulations are shown in Fig. 4. The success rate is the percentage of runs (out of the 135 total per object) that successfully deliver the object to the goal without it being dropped from the tray. The Robust constraints are always successful (with a maximum object displacement of only 2 mm). The Top and Center constraints produce fewer successful runs as the object height increases, which suggests that the sticking constraints are more sensitive to parameter error for taller objects. The success rate of the Top and Center constraints varies slightly when using more SQP iterations  $n_s$  to solve (7), at the cost of a longer solve time. We report the results for  $n_s = 3$  and  $n_s = 10$  (the Robust constraints are completely successful for both values of  $n_s$ , so we only report  $n_s = 3$ ); increasing to  $n_s = 20$  did not produce a higher success rate. The average solve times for the Center constraints are 110 ms ( $n_s = 3$ ) and 310 ms ( $n_s = 10$ ); for the Top constraints 111 ms ( $n_s = 3$ ) and 324 ms ( $n_s = 10$ ); and for the Robust constraints 324 ms. Even when more compute

Table I: Maximum constraint violation for each object height and sticking constraint method using the moment conditions for physical realizability. A negative value means that the constraints are never violated for any realizable inertial parameters, which is only the case using our proposed Robust constraints. These results are for  $n_s = 3$ ; the values with  $n_s = 10$  are very similar.

Height [cm]	Center	Top	Robust
30	2.48	4.51	-1.15
40	5.03	7.19	-0.97
50	8.21	9.09	-0.77
60	11.96	10.50	-0.56

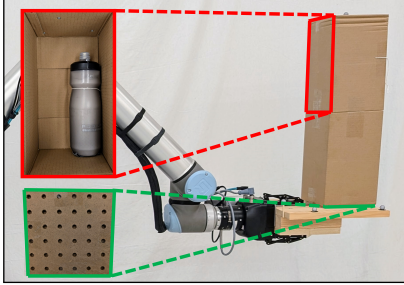


Figure 5: Our transported objects are boxes containing a bottle filled with sugar to offset the CoM and to make the task of balancing more difficult. One cannot tell how the box is packed (and therefore what its mass distribution is) just by looking at it. Box2 (shown on the right) consists of two boxes attached together; Box1 is a single box. A firm base board (green) is attached to the bottom box to provide a consistent contact area with the tray.

time is used to refine the trajectory, the baselines are still not as successful as the Robust constraints.

While the results in Fig. 4 show that our proposed constraints are robust for *particular* combinations of CoM positions and inertia matrices, Table I shows the maximum possible sticking constraint violations for *any* realizable inertial parameter value, obtained by solving (12) at each point along the planned trajectory (discretized with a 10 ms interval). Solving (12) for all  $i = 1, \dots, n_h$  at a single timestep took about 2.2 s. The Robust constraints have no violation for any possible value of the inertia matrix (while the Center and Top constraints always do), justifying our decision to ignore uncertainty in the inertia matrix within the planner. While negative violation implies failure should not occur; positive violation does not mean that it *will* occur.

Finally, recall that the simulated value of the friction coefficient between the tray and object is  $\mu = 0.2$ . This value does not impact the behavior of the planner because the planner assumes  $\mu = 0$  and then tries to satisfy the softened sticking constraints approximately. However, the underlying value of  $\mu$  can potentially affect the amount of constraint violation, since  $h_i$  in (12) depends on the friction coefficient. Interestingly, we evaluated the constraint violation for the robust constraints with  $h = 60$  cm and  $\mu = 0.1$  and found the maximum constraint violation to be the same as with  $\mu = 0.2$ , which suggests that the friction coefficient is not the limiting factor when transporting tall objects like those used here.

## IX. HARDWARE EXPERIMENTS

We also perform experiments on our real mobile manipulator balancing a cardboard box, as shown in Fig. 1. We test two heights of box, Box1 and Box2, each containing a bottle

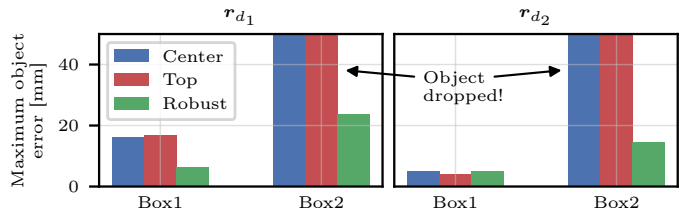


Figure 6: Maximum object displacement error for the different constraint methods, desired positions, and box objects. The object displacement error is the maximum distance the object moves from its initial position relative to the tray. The errors are similar between each method with Box1 (the shorter box), but the Center and Top baselines fail with Box2 (the taller box), while the proposed Robust constraints successfully transport it.

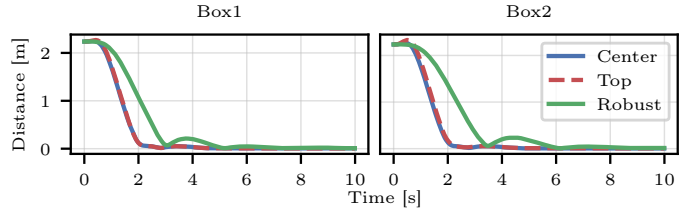


Figure 7: Distance between the EE position and the desired position over time for desired position  $r_{d_1}$  and each sticking constraint method. The trajectories with the Center and Top constraints, in which only a single CoM value is considered, are nearly the same. The Robust constraints result in slower convergence, but always successfully transport the object.

filled with sugar in one corner to offset the CoM (see Fig. 5). Box1 has a height of  $h_1 = 28$  cm and a square base with side length 15 cm. Its total mass is 933 g, with the bottle contributing 722 g. Box2 is made of two stacked boxes attached together, with the top one containing the bottle. Its total mass is 1046 g and its height is  $h_2 = 56$  cm; its base dimensions are the same as Box1. A rigid board is attached to the base of the boxes to ensure consistent contact with the tray (again, refer to Fig. 5). The friction coefficient between the boxes (with the attached base board) and the tray was experimentally measured to be  $\mu = 0.29$ . Position feedback is provided for the arm by joint encoders at 125 Hz and for the base by a Vicon motion capture system at 100 Hz. The laptop specifications and planner parameters are the same as in simulation. The control loop is run at the arm's control frequency of 125 Hz.

We consider the scenario when the planner does not know how the box is packed, and therefore its inertial parameters are not known exactly. We again test the Center, Top, and Robust constraints using the desired positions  $r_{d_1}$  and  $r_{d_2}$ .<sup>3</sup> The Robust constraints assume the CoM lies in the cuboid  $\mathcal{C}$  with dimensions  $12 \text{ cm} \times 12 \text{ cm} \times h_i$ , where  $i = 1, 2$  corresponds to Box1 or Box2, which is large enough to contain any possible centroid of the bottle no matter its position in the box. We perform up to three runs of each combination of desired position and constraint method; if a given combination fails before completing three runs, we stop to avoid extra damage to the boxes. Using  $n_s = 3$ , each of the constraint methods successfully transported Box1 for three runs, but only the Robust constraints were able to do so with Box2 (with either  $n_s = 3$  and  $n_s = 10$ ). With both values of  $n_s$ , the Center constraints failed immediately with  $r_{d_1}$ , and completed one

<sup>3</sup>We did not use the desired position  $r_{d_3}$  because in that case if the box falls, it falls onto the robot, possibly causing damage.

Table II: The maximum planned EE velocity and acceleration as well as the root-mean-square tracking error of the arm’s joint angles and the base’s position and yaw angle in the hardware experiments.

	Box1			Box2		
	Center	Top	Robust	Center	Top	Robust
EE max. vel. [m/s]	2.32	2.36	1.27	2.36	2.43	1.08
EE max. acc. [m/s <sup>2</sup> ]	4.24	4.46	1.17	4.46	4.88	0.87
Arm err. [deg]	0.38	0.37	0.22	0.39	0.33	0.21
Base pos. err. [cm]	2.67	2.82	1.96	2.56	3.16	1.48
Base yaw err. [deg]	1.80	1.90	0.62	1.68	2.25	0.31

run of  $r_{d_2}$  before dropping the box on the second run; the Top constraints failed immediately for both desired positions. The maximum object displacement errors (for  $n_s = 3$ ) are shown in Fig. 6. The Robust constraints produce smaller errors with both Box1 and Box2 (there is still *some* error, due to unmodelled effects like vibrations, drag, and inevitable model inaccuracies); the Center and Top baselines obviously produce large errors with Box2 since the box was dropped. The planning times were similar to those in simulation.

The convergence of the EE to the desired position for  $r_{d_1}$  is shown in Fig. 7 and additional metrics are in Table II. While the Center and Top constraint methods converge faster, this comes with the risk of dropping uncertain objects, especially taller ones like Box2. While the Robust constraints still produce fast motion, the maximum velocity and acceleration is reduced compared to the baselines. The root-mean-square tracking error (RMSE) for the arm is quite low, which suggests that neglecting the object mass was reasonable. The RMSE for the base is higher, suggesting that adding mobility to the waiter’s problem requires additional robustness to error.

## X. CONCLUSION

We present a planning framework for nonprehensile object transportation that is robust to uncertainty in the transported object’s inertial parameters. In particular, we explicitly model and design robust constraints for uncertainty in the object’s CoM, and demonstrate successful transportation of tall objects in simulation and on real hardware. We also use moment relaxations to develop conditions for the inertial parameters of the transported object to be physically realizable, which allows us to determine if the constraints would be violated for *any* possible value of the inertial parameters, including the inertia matrix, along the planned trajectories.

## REFERENCES

- [1] F. G. Flores and A. Kecskeméthy, “Time-optimal path planning for the general waiter motion problem,” in *Advances in Mechanisms, Robotics and Design Education and Research*, 2013, pp. 189–203.
- [2] K. M. Lynch, “Nonprehensile robotic manipulation: Controllability and planning,” Ph.D., Carnegie Mellon University, 1996.
- [3] A. Heins and A. P. Schoellig, “Force push: Robust single-point pushing with force feedback,” *IEEE Robotics and Automation Letters*, vol. 9, no. 8, pp. 6856–6863, 2024.
- [4] F. Ruggiero, V. Lippiello, and B. Siciliano, “Nonprehensile dynamic manipulation: A survey,” *IEEE Robotics and Automation Letters*, vol. 3, no. 3, pp. 1711–1718, 2018.
- [5] Q.-C. Pham, S. Caron, P. Lertkultanon, and Y. Nakamura, “Admissible velocity propagation: Beyond quasi-static path planning for high-dimensional robots,” *Int. J. Robotics Research*, vol. 36, no. 1, pp. 44–67, 2017.
- [6] A. Heins and A. P. Schoellig, “Keep it upright: Model predictive control for nonprehensile object transportation with obstacle avoidance on a mobile manipulator,” *IEEE Robotics and Automation Letters*, vol. 8, no. 12, pp. 7986–7993, 2023.
- [7] S. Traversaro, S. Brossette, A. Escande, and F. Nori, “Identification of fully physical consistent inertial parameters using optimization on manifolds,” in *Proc. IEEE/RSJ Int. Conf. Intelligent Robots and Systems*, 2016, pp. 5446–5451.
- [8] P. M. Wensing, S. Kim, and J.-J. E. Slotine, “Linear matrix inequalities for physically consistent inertial parameter identification: A statistical perspective on the mass distribution,” *IEEE Robotics and Automation Letters*, vol. 3, no. 1, pp. 60–67, 2018.
- [9] J. B. Lasserre, *Moments, positive polynomials and their applications*. World Scientific, 2009.
- [10] C. Zhou, M. Lei, L. Zhao, Z. Wang, and Y. Zheng, “TOPP-MPC-based dual-arm dynamic collaborative manipulation for multi-object nonprehensile transportation,” in *Proc. IEEE Int. Conf. Robotics and Automation*, 2022, pp. 999–1005.
- [11] H. Gattringer, A. Müller, S. Weitzhofer, and M. Schörgenhuber, “Point to point time optimal handling of unmounted rigid objects and liquid-filled containers,” *Mechanism and Machine Theory*, vol. 184, p. 105286, 2023.
- [12] Z. Brei, J. Michaux, B. Zhang, P. Holmes, and R. Vasudevan, “Serving time: Real-time, safe motion planning and control for manipulation of unsecured objects,” *IEEE Robotics and Automation Letters*, vol. 9, no. 3, pp. 2383–2390, 2024.
- [13] M. Selvaggio, A. Garg, F. Ruggiero, G. Oriolo, and B. Siciliano, “Non-prehensile object transportation via model predictive non-sliding manipulation control,” *IEEE Trans. Control Systems Technology*, pp. 1–14, 2023.
- [14] L. Moriello, L. Biagiotti, C. Melchiorri, and A. Paoli, “Manipulating liquids with robots: A sloshing-free solution,” *Control Engineering Practice*, vol. 78, pp. 129–141, 2018.
- [15] R. I. C. Muchacho, R. Laha, L. F. C. Figueredo, and S. Haddadin, “A solution to slosh-free robot trajectory optimization,” in *Proc. IEEE/RSJ Int. Conf. Intelligent Robots and Systems*, 2022, pp. 223–230.
- [16] M. Selvaggio, J. Cacace, C. Pacchierotti, F. Ruggiero, and P. R. Giordano, “A shared-control teleoperation architecture for nonprehensile object transportation,” *IEEE Trans. Robotics*, vol. 38, no. 1, pp. 569–583, 2022.
- [17] R. Subburaman, M. Selvaggio, and F. Ruggiero, “A non-prehensile object transportation framework with adaptive tilting based on quadratic programming,” *IEEE Robotics and Automation Letters*, pp. 1–8, 2023.
- [18] S. Caron, Q.-C. Pham, and Y. Nakamura, “Leveraging cone double description for multi-contact stability of humanoids with applications to statics and dynamics,” in *Proc. Robotics: Science and Systems*, 2015.
- [19] S. Caron and A. Kheddar, “Multi-contact walking pattern generation based on model preview control of 3D COM accelerations,” in *Proc. IEEE-RAS Int. Conf. Humanoid Robots*, 2016, pp. 550–557.
- [20] N. Giftsun, A. D. Prete, and F. Lamiroux, “Robustness to inertial parameter errors for legged robots balancing on level ground,” in *Proc. Int. Conf. Informatics in Control, Automation and Robotics*, 2017.
- [21] X. Jiang, W. Chi, Y. Zheng, S. Zhang, Y. Ling, J. Xu, and Z. Zhang, “Locomotion generation for quadruped robots on challenging terrains via quadratic programming,” *Autonomous Robots*, vol. 47, no. 1, pp. 51–76, 2023.
- [22] H. Yang and L. Carlone, “Certifiably optimal outlier-robust geometric perception: Semidefinite relaxations and scalable global optimization,” *IEEE Trans. Pattern Analysis and Machine Intelligence*, vol. 45, no. 3, pp. 2816–2834, 2023.
- [23] S. Kang, X. Xu, J. Sarva, L. Liang, and H. Yang, “Fast and certifiable trajectory optimization,” in *Proc. Workshop Algorithmic Foundations of Robotics*, 2024.
- [24] D. J. Balkcom and J. Trinkle, “Computing wrench cones for planar rigid body contact tasks,” *Int. J. Robotics Research*, vol. 21, no. 12, pp. 1053–1066, 2002.
- [25] K. Fukuda and A. Prodon, “Double description method revisited,” in *Proc. Combinatorics and Computer Science*, 1996, pp. 91–111.
- [26] M. T. Mason and K. M. Lynch, “Dynamic manipulation,” in *Proc. IEEE/RSJ Int. Conf. Intelligent Robots and Systems*, 1993, pp. 152–159.
- [27] “OCS2: An open source library for optimal control of switched systems.” [Online]. Available: <https://github.com/leggedrobotics/ocs2>
- [28] G. Frison and M. Diehl, “HPIPM: a high-performance quadratic programming framework for model predictive control,” *IFAC-PapersOnLine*, vol. 53, no. 2, pp. 6563–6569, 2020.